ACS OMEGA

http://pubs.acs.org/journal/acsodf

Article

Transient Destabilization of Biological Membranes Contributes to the Superior Performance of Star-Shaped PDMAEMA in Delivering pDNA

Valérie Jérôme, Christopher V. Synatschke, and Ruth Freitag*

Cite This: *ACS Omega* 2020, 5, 26640−26654

Read Online

ACCESS | Metrics & More | Article Recommendations

ABSTRACT: Nonviral DNA vectors are promising alternatives to viral ones. Their use in DNA medicine is limited by an inability to transfect, for example, nondividing or suspension cells. In recent years, star-shaped synthetic polycationic vectors, so called "Nanostars", have shown some promise in this regard, at least when compared to the "gold standard" in nonviral vectors, namely, linear poly(ethyleneimine) (l-PEI). It has been hypothesized that an ability to transiently destabilize cellular membranes is partially responsible for the phenomenon. This hypothesis is investigated here, taking human leukemia suspension cells (Jurkat cells) as an example. Contrary to l-PEI, the Nanostars promote the cellular uptake of small, normally membrane-impermeant molecules (trypan blue and propidium iodide) as well as that of fluorescent polystyrene beads (average diameter 100 nm). Since Nanostars, but not l-PEI, are apparently able to deliver DNA to nuclei of nondividing cells, nuclear uptake is, in addition, investigated with isolated cell nuclei. Our results provide evidence that Nanostars are more efficient than l-PEI in increasing the nuclear membrane association/permeability, allowing accumulation of their cargo on/in the nucleus.

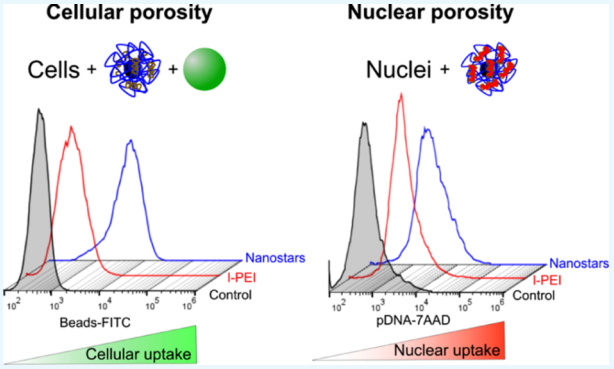

INTRODUCTION

Synthetic polycations represent promising and affordable DNA vectors for gene delivery. They already play an important role in research and development, for example, in the preparation of recombinant mammalian production cell lines in the biopharmaceutical industry. Certain advantages of nonviral over viral agents argue for a corresponding potential in DNA medicine, for example, their versatility, their safety, their relatively low production cost, and their low immunogenicity.[1] However, the application range of nonviral vectors in this regard is still limited. For example, nondividing and suspension cells have been found "difficult-to-transfect" by nonviral agents.[2−4]

An important task for a polycationic nonviral gene delivery agent is the compaction and charge overcompensation of the negatively charged plasmid DNA (pDNA), thereby forming stable positively charged polyelectrolyte complexes ["polyplexes" (PPs)]. In order to assure that the formed PPs bear a positive net-charge and therefore are attracted by the negatively charged cellular surface, PP formation and transfection typically require a surplus of polycations. Poly(ethyleneimine) (PEI) is one of the most efficient polycationic vectors described to date because of its high density of positively charged amines.[5−7] In recent years, we and other researchers have demonstrated the potential of poly(2-(*N*,*N*′-dimethylamino)ethyl methacrylate) (PDMAEMA) as an alternative polycationic gene therapy vector.[8−13]

Despite considerable progress, important aspects of the various stages of nonviral gene delivery remain poorly understood and hence difficult to improve. This includes, besides cellular uptake, also intracellular transport and finally nuclear uptake (for a recent review, see Durymanov 2018[14]). Moreover, the dominating mechanisms at each stage may vary as a function of vector architecture, polyplex size and density,[15] as well as the cell type.[16] Positively charged PPs may, for example, be taken up by the cells via both clathrin- and caveolae-meditated endocytosis,[17−19] which, however, are limited to objects with sizes <300 and <80 nm, respectively.[20−22] All forms of endocytosis also suffer from a low percentage of endosomal escape.[23−25] Hence, nucleic acids delivered by endocytosis are often trapped in the endosome

Received: July 21, 2020
Accepted: September 17, 2020
Published: October 5, 2020

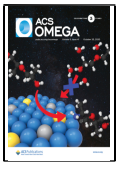

https://dx.doi.org/10.1021/acsomega.0c03367
ACS Omega 2020, 5, 26640−26654

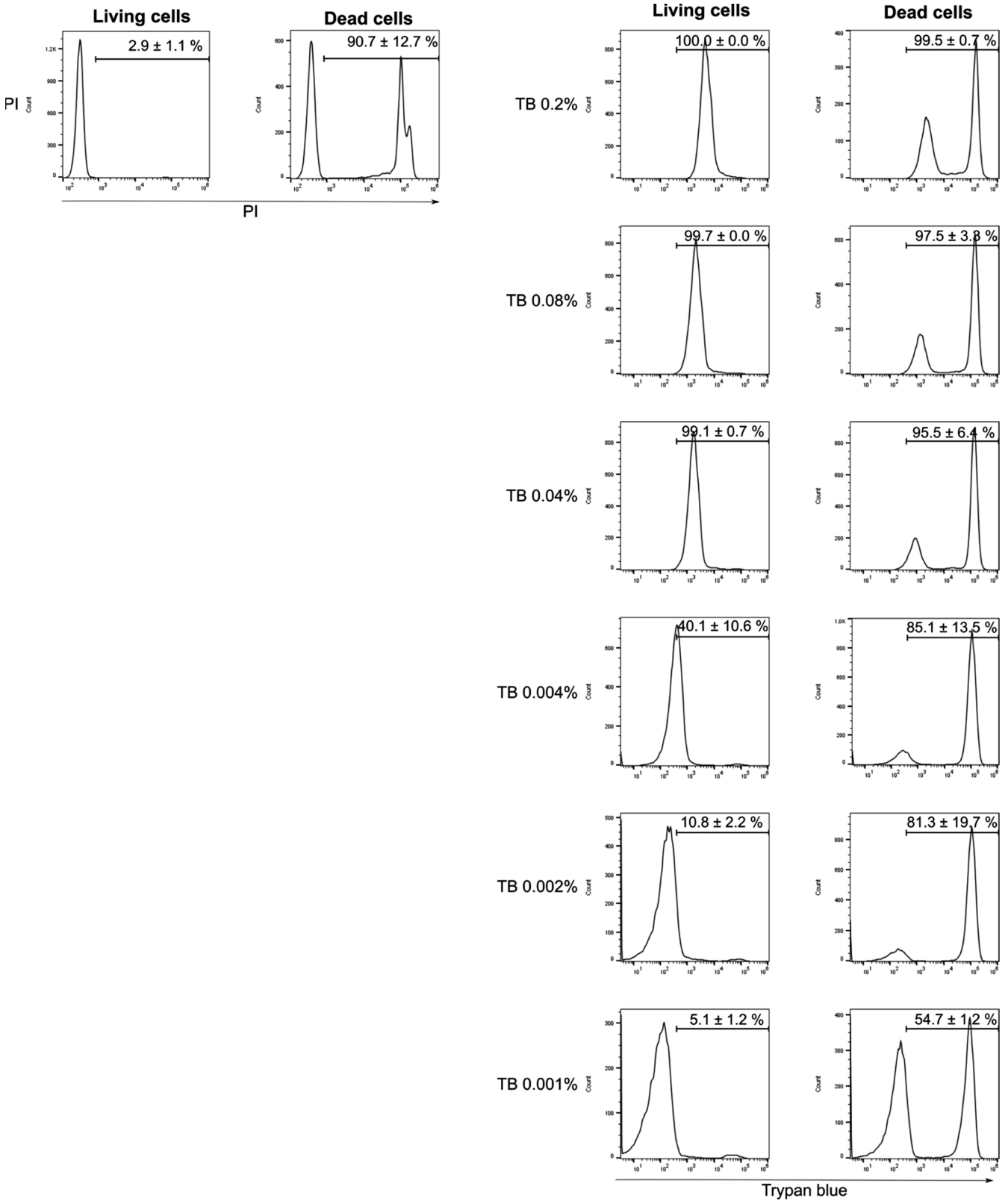

Figure 1. Evaluation of trypan blue (TB) concentrations ranging from 0.2 to 0.001% to discriminate between living and dead cells. Staining with propidium iodide (PI) was used as a reference. Living cells: Jurkat cells collected in the exponential growth phase. Dead cells: Jurkat cells incubated for 45 min at 50 °C in a water bath. For both PI- and TB-treated cells, 20,000 events were acquired. Data represent representative histograms of the flow cytometry analysis and mean ± SD, n = 3 for PI and TB positive cells.

and subsequently recycled to the plasma membrane or trafficked to multivesicular bodies for degradation in lysosomes, leading to low transfection efficiency.[26] However, some transfection agents are capable of endosomal release.[3,27] Polycations (e.g., PEI) with high buffering capacity can be protonated under the acidic environment of the endosome.[28]

https://dx.doi.org/10.1021/acsomega.0c03367
ACS Omega 2020, 5, 26640−26654

This protonation increases endosomal pH and induces extensive ionic transportation into the endosome, resulting in the rupture of the endosomal membrane and the release of the trapped cargoes, that is, the controversial "proton-sponge effect" hypothesis.[29] In the acidic endosomal environment, dedicated molecules can also adopt an amphipathic conformation and interact with the lipid bilayer of the endosome, causing an internal stress sufficiently strong to create pores.[30] Most current methods for studying internalization of particles (e.g., PPs) involve exclusion of specific endocytic mechanisms, using inhibitors of endocytosis. However, many, if not all, of these inhibitors act in a nonspecific cell type-dependent manner, disturbing cellular processes, and thus suffer from unknown global effects on the cell, making their use and the interpretation of the findings debatable.[31−33]

Regardless of the mechanism for cellular uptake and intracellular transport, the simple fact that nonviral vectors are generally unable to transfect nondividing cells argues that the nuclear membrane poses a severe barrier to DNA delivery in their case.[17] The nuclear envelope is impermeable to molecules >40 kDa (corresponding to a hypothetical 60 bp DNA).[34] Nucleocytoplasmic transport across the nuclear membrane is possible by nuclear pore complexes (NPCs) but is also restricted by an estimated cutoff in size of approximately 5 nm[35] due to the size limitation posed by the NPC itself (i.e., a central channel diameter of ∼45−50 nm),[27,36−38] which renders the ingress of nanoparticles or macromolecules extremely difficult.[39,40] It is therefore commonly accepted that successful nonviral DNA transfection is limited to actively dividing cells.[41,42] In this case, the transgene can access the nuclear region during cell division, when the nuclear envelope temporarily breaks down.[43] Alternatively, nonviral delivery systems have been designed to include various types of "facilitators" (e.g., coupling nuclear localization signals or incorporating transcription factor binding sequences to pDNA) to improve nuclear delivery.[3,4,42,44] However, these approaches are technically demanding and have sometimes met with limited success in terms of an improvement of the transgene expression.

In this context, reports from several groups including our own are of interest, which show efficient gene delivery into nondividing cells using plain nonviral polymeric systems.[11,45−47] These reproducibly obtained results implicate a not yet elucidated mechanism for penetrating the nucleus in the presence of the nuclear envelope. Moreover, we showed that the star-shaped PDMAEMA ("Nanostar") developed in recent years in our group is, in addition, also able to efficiently transfect other types of a notoriously hard-to-transfect cells, such as suspension cells, most notably Jurkat cells, that is, cells from a lymphoblastic leukemia cell line which is a widely used model for human T lymphocytes.[11] Under optimized conditions, >80% transfection efficiency while preserving 80% cellular viability was reproducibly obtained, which is an order of magnitude higher than with linear poly(ethyleneimine) (l-PEI) in terms of transfection efficiency and twice as good in terms of viability.[12] The mechanistic basis for these differences is still unknown. Hypotheses based on differences in the mechanisms of cellular and/or nuclear entry have been proposed, largely based on studies from Orr's group, which showed that polycations are able to transiently disrupt and induce nanopores in synthetic lipid bilayer structures and in natural cellular membranes.[48−51]

The present contribution investigates the hypothesis that the superior DNA delivery ability of the Nanostars relies on a mechanism for transient poration of initially the plasma and later the nuclear membrane, which differs from the effect exerted by l-PEI on these membranes and is both more conductive to gene delivery and less toxic for the cells. By using combinations of small molecular probes typically used for dye exclusion assays [propidium iodide (PI) and trypan blue (TB)] as well as fluorescently labeled pDNA and polystyrene (PS) beads, the influence of polycation chemistry and architecture on the permeation of the cellular and nuclear membranes is investigated.

RESULTS AND DISCUSSION

Determination of the Optimum TB Concentration for the Porosity Assay in Jurkat Cells. TB (873 Da) and PI (668 Da) were chosen to test for nanopore formation during polycation-based transfection since these molecules are known to be incapable of passing an intact cellular membrane. In fact, these dyes are normally used to identify dead cells, where the cellular membrane becomes leaky. TB emits fluorescence when complexed with proteins,[52] while PI intercalates in double helices formed by polynucleotides and then gives a bright red fluorescence.[53]

When Brito-Melo's group developed a flow cytometry-based TB exclusion assay for dead cells,[54] they stressed the importance of determining the optimum TB concentration to distinguish between living cells, which still have a basal fluorescence level due to the TB−protein interaction on the cellular surface, from the dead cells, where TB−protein complexation occurs both on the cellular surface and in the cytoplasm.

To accommodate these requirements in our investigation, different TB concentrations were tested to evaluate the optimum experimental condition for distinguishing between fluorescence emitted by living and dead cells after contact with TB (Figure 1). PI staining restricted to dead cells under these conditions was performed as the control. From these results, we deduced that cells with median fluorescence intensity (MFI) < 10^3 au can be classified as "alive" and cells with MFI ≥ 3×10^4 au as "dead". A final concentration of 0.001% (w/v) TB in the assay was able to distinguish dead (stained; MFI ≥ 3×10^4 au) cells, keeping live ("unstained") cells in a negative region usually located between 100 and 10^3 au on FL4-based histograms. This concentration was therefore considered suitable for the determination of TB ingress into living cells after membrane destabilization during or due to the transfection process and was used for all further experiments.

Evaluation of the Polyplex Fluorescence after Incubation with TB or PI. A priori, an unspecific and undesirable direct interaction between TB/PI and either l-PEI or Nanostars, could not be excluded. Therefore, we first evaluated the fluorescence emitted by the free polymers and their respective PPs (N/P 20, l-PEI, PP_{PEI}; N/P 10, Nanostar, $PP_{Nanostar}$) after incubation for 20 min with TB (0.001%) or PI (1 $\mu g\ mL^{-1}$), Table 1.

As expected, after incubation with PI, both types of PPs, but not the respective free polymer, displayed a detectable fluorescence due to the incorporation of PI into the complexed pDNA. However, this fluorescence was 4- to 6-fold lower than the fluorescence recorded for similar amounts of free pDNA (fluorescence: 40,677 ± 3625), indicating that the accessibility of pDNA for PI was restricted in the PPs.

https://dx.doi.org/10.1021/acsomega.0c03367
ACS Omega 2020, 5, 26640−26654

Table 1. Overview of Fluorescence of Free Polymers and PPs after Incubation with TB or PI[a]

	fluorescence (au)			
	l-PEI		Nanostar	
	polymer	polyplex	polymer	polyplex
PI	b.d.	9964 ± 358	b.d.	6902 ± 538
TB	784 ± 258	1076 ± 177	27,438 ± 3556	22,052 ± 4528

[a]PPs were built in HBG at N/P 10 (Nanostar) and 20 (l-PEI). Fluorescence PI was measured at Ex: 535 ± 20 nm/Em: 612 ± 20 nm. Fluorescence TB was measured at Ex: 485 ± 20 nm/Em: 670 ± 20 nm. b.d.: below detection limit (similar to blank). The values represent ($F_{sample} - F_{blank}$) with $F_{blank,TB}$: 7551 ± 1019 and $F_{blank,PI}$: 2408 ± 249. Mean ± SD, n = 4.

After incubation with TB, the fluorescence values were low in the case of l-PEI or l-PEI-PPs, whereas high fluorescence values were detected for both free Nanostars and the corresponding PPs. Considering that the fluorescence value of the free pDNA was also low in the presence of TB (fluorescence: 3041 ± 538), these results indicate that TB can interact with the Nanostar molecules leading to high fluorescence. Since both polycations contain very similar amine groups, but differ significantly in hydrophobicity, hydrophobic interactions between TB and the Nanostars may be the cause for the unexpected high fluorescence observed in the case of the Nanostars. As a consequence, a piggybacking of the TB dye on Nanostars should be borne in mind during further data discussion of TB cellular uptake.

Porosity Assay in the six-Well Transfection Protocol. In order to follow the extent of a putative destabilization of the

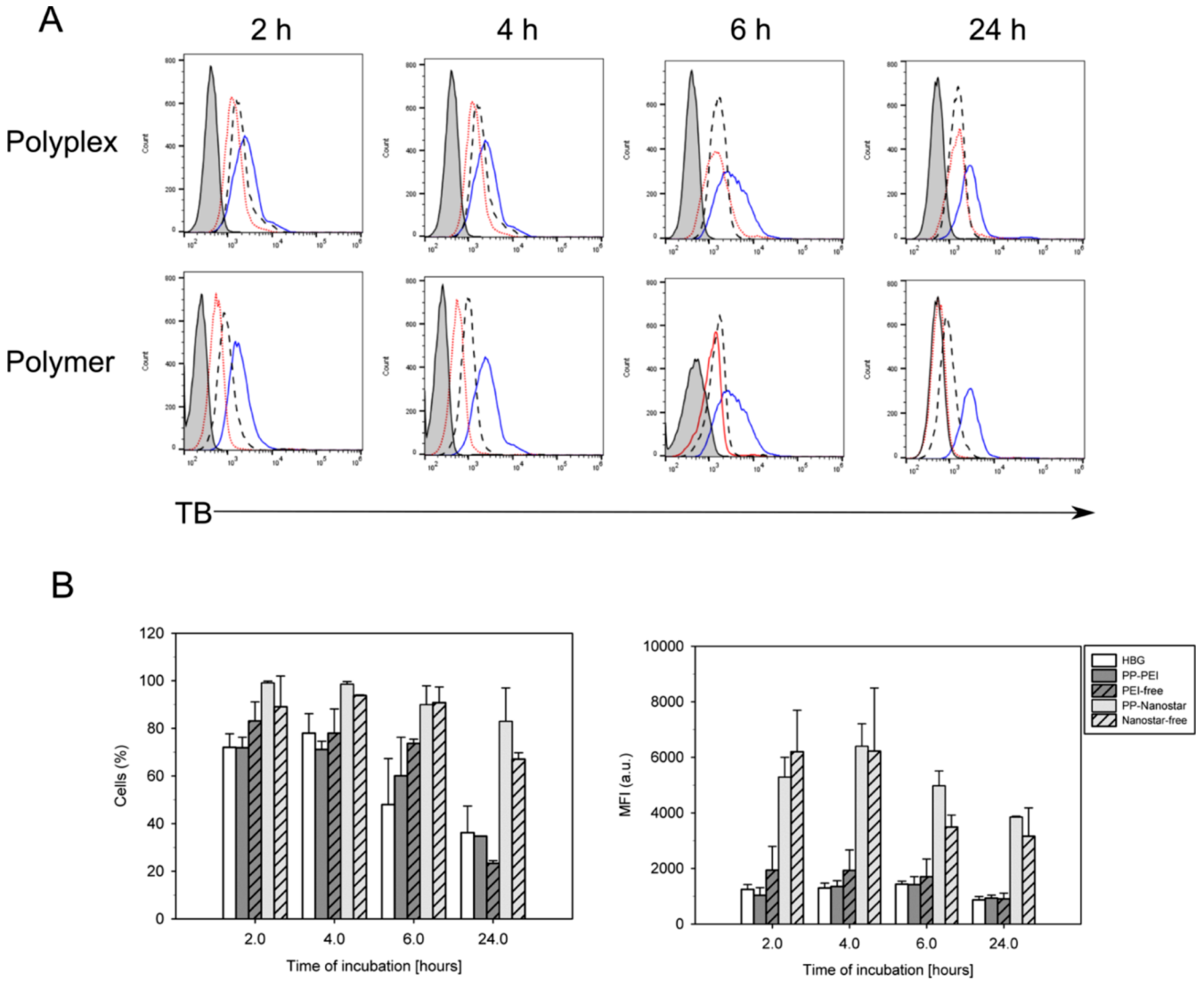

Figure 2. Cellular uptake of TB by Jurkat cells during standard transfections in six-well plates. Development of the TB positive cell fraction after incubation with l-PEI (PP-PEI) and Nanostar-based (PP-Nanostar) PPs or a corresponding amount of free polymers (PEI_{free}, $Nanostar_{free}$). Cells (1×10^5 cells mL^{-1}) were incubated in six-well plates (total incubation volume: 2.2 mL) with 2.3 μg mL^{-1} (l-PEI, N/P 20) and 4.5 μg mL^{-1} (Nanostar, N/P 10). The first 4 h corresponds to incubation of the cells in Opti-MEM (serum-free conditions) containing 0.001% TB. Thereafter, the medium was exchanged for R10 (10% serum) without TB supplementation. (A) Representative overlays of TB fluorescence. Grey, control cells (incubation without TB); black dashed line, HBG; red dotted lines, l-PEI; blue solid lines, Nanostar. (B) Results from the flow cytometry were expressed either as percentages of cells positive for TB-fluorescence in the forward scatter (FSC)/side scatter (SSC) nonapoptotic gate (left side) or median fluorescence for TB-positive gated cells (right side). Data points represent mean ± SD, $n \geq 2$.

https://dx.doi.org/10.1021/acsomega.0c03367
ACS Omega 2020, 5, 26640−26654

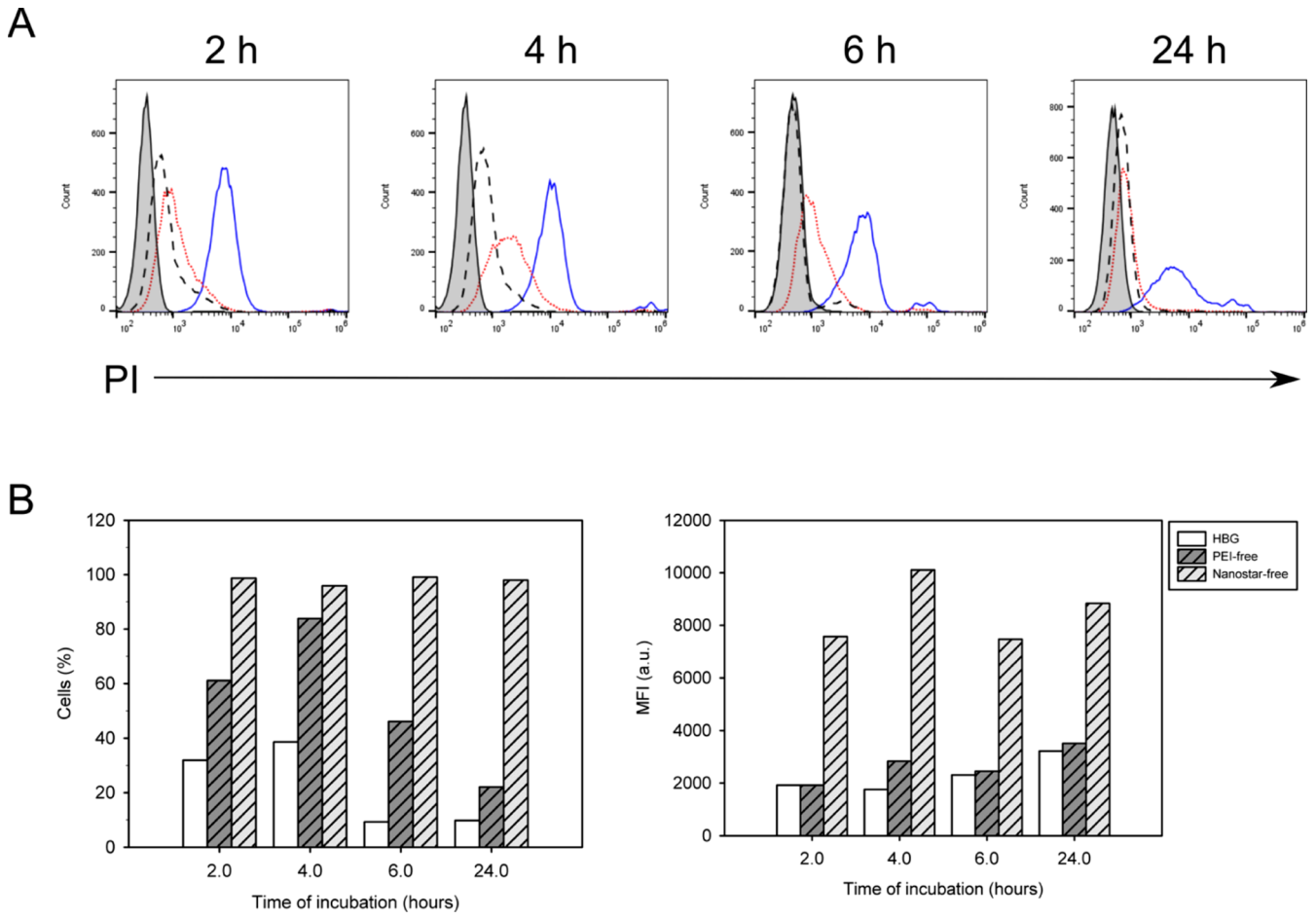

Figure 3. Cellular uptake of PI by Jurkat cells during standard transfections in six-well plates. Development of the PI positive cell fraction after incubation with free polymers (PEI_{free}, $Nanostar_{free}$). Cells (1×10^5 cells mL^{-1}) were incubated in six-well plates (total incubation volume: 2.2 mL) with 2.3 μg mL^{-1} (l-PEI) and 4.5 μg mL^{-1} (Nanostar). The first 4 h corresponds to incubation of the cells in Opti-MEM (serum-free conditions) containing 1 μg mL^{-1} PI. Thereafter, the medium was exchanged for R10 (10% serum) without PI supplementation. (A) Representative overlays of PI fluorescence. Grey, control cells (incubated without PI); black dashed line, HBG; red dotted lines, l-PEI; blue solid lines, Nanostar. (B) Results from the flow cytometry were expressed either as percentages of cells positive for PI-fluorescence in the FSC/SSC nonapoptotic gate (left side) or median fluorescence for PI-positive gated cells (right side). Data points represent one experiment performed in duplicates.

cellular membrane under transfection conditions, we first performed standard transfections of Jurkat cells in six-well plates (l-PEI N/P 20, Nanostar: N/P 10) in the presence of 0.001% TB and followed the development of the TB fluorescence by flow cytometry for up to 24 h. Aliquots of the cells were, in addition, put through a mock transfection (i.e., a polymer without pDNA) for each polycation. Cells solely incubated with the complexation buffer, namely HBG, and TB served as negative controls.

Incubation of the cells with TB in the presence of the PPs for 2 or 4 h (i.e., up to the medium exchange) resulted in 70% fluorescent cells in the case of l-PEI, while in the case of Nanostars, almost 100% of the nonapoptotic cells stained positive for TB, Figure 2. Similar results were obtained for the mock transfections performed with just the free polycations, whereas the percentage of TB-positive cells in the negative controls (incubation in just the HBG/TB mixture and no added polycation) was also 70%, that is, in the same range as for l-PEI. The results from the negative control (HBG group) can be considered as the background level of staining most likely caused by an association of TB with proteins in the cellular membrane, only occurring after extended incubation (for comparison see cells incubated for 5 min with TB, Figure 1).

More pronounced differences were seen in terms of the MFI, Figure 2B (right side), where the MFI of the l-PEI and HBG groups was similar and significantly lower than that of the Nanostar groups. As shown above (Table 1), TB can interact with Nanostars leading to high fluorescence emission. Beside direct interactions of TB molecules with the cellular membrane and intracellular proteins, a piggybacking on Nanostars might also be responsible for the high MFI observed after incubation with Nanostars in a free or complexed form. In all cases, differences between the values of the PPs and those of the corresponding free polymers were not statistically significant ($p < 0.05$). Taken together, these results suggest that there is a distinct difference in the behavior of the Nanostar versus l-PEI in terms of membrane permeabilization and that the surplus of polymers typically found in transfection cocktails is at least partly responsible for this.

Moreover, there is a striking similarity in the development of the TB fluorescence in the case of the negative controls and the l-PEI group. For instance, 2 h after exchange of the transfection mixture for fresh R10 (recovery period, time

https://dx.doi.org/10.1021/acsomega.0c03367
ACS Omega 2020, 5, 26640−26654

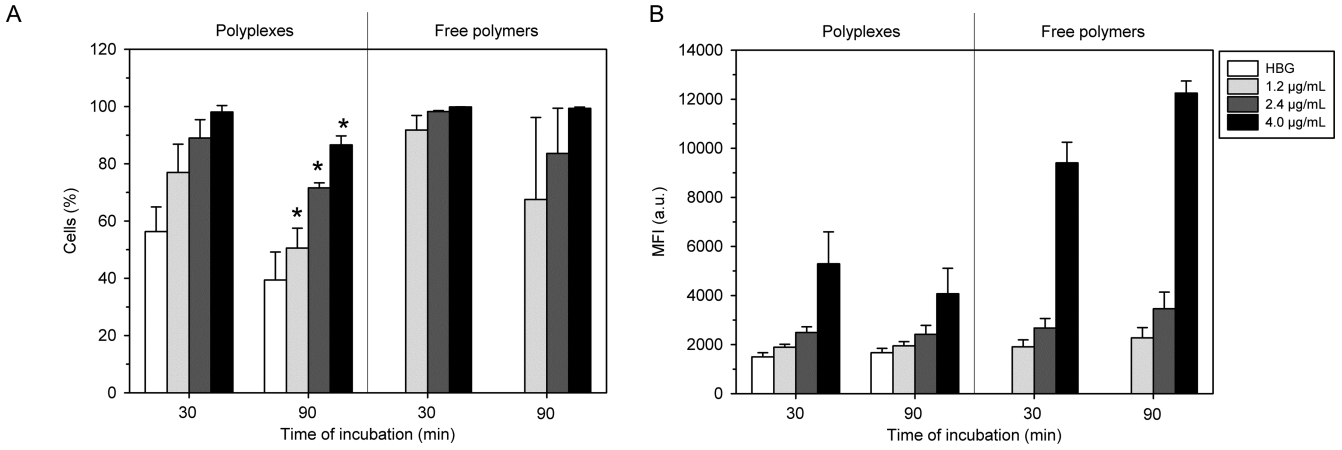

Figure 4. Cellular uptake of TB by Jurkat cells during transfection in microtubes. Cells (4×10^5 cells mL^{-1}) were incubated for 30 to 90 min in microtubes (total incubation volume: 0.5 mL; Opti-MEM (serum-free conditions)) with the PP-Nanostar built at N/P 10 with the indicated polymer concentrations or the corresponding amount of free polymers in the presence of 0.001% TB. Cells incubated with HBG served as the negative control. Flow cytometry results were expressed either as percentages of cells positive for TB-fluorescence in the FSC/SSC nonapoptotic gate (A) or median fluorescence for TB-positive gated cells (B). Data points represent mean ± SD, $n \geq 2$. *: statistically significant between the 30 min and the 90 min groups, $p < 0.05$.

point: 6 h), a nonsignificant decrease of the percentage of TB-positive cells was observed for HBG- and l-PEI-treated cells. This trend is confirmed after 24 h incubation in fresh R10 with less than 30% of the HBG- and PEI-treated cells still testing TB-positive. Such a dramatic reduction of the number of TB-positive cells after media exchange could easily be due to a displacement of TB molecules from cell membrane proteins to serum proteins of the growth medium. Hence, this is an indication that in such cases, TB is not taken up in larger quantities by the cells but mainly been bound to the surface. Since Jurkat cells are suspension cells, the direct distinction between attached and incorporated TB, for example by confocal microscopy, is made difficult because these cells do not readily attach to substrates in a manner needed for imaging. We are currently investigating a variety of coating methods such as fibronectin and poly-L-lysine for cell immobilization[55] but still face technical difficulties, which result in unsatisfactory reproducibilities of the experimental results.

In the case of Nanostars (free polymer/polyplex)-treated cells, the percentage of TB-positive cells dropped only slightly with time and was still >80% ($PP_{Nanostar}$) and >65% (free Nanostar) 24 h after medium change. MFI values above those recorded for the negative controls could also only be detected in the Nanostar groups. The observed 1.5-fold decrease of the MFI with time could be due in part to a displacement of extracellularly bound TB molecules by serum proteins, as discussed above, but also to a dilution of intracellular TB during cell division.

The results obtained for the Nanostar may thus be explained by pore formation in the membrane and also by piggybacking of the TB on the polycation, when the polymers/PPs are taken up by the cells by mechanisms such as endocytosis. To further discriminate between these possibilities, we repeated the experiments using PI as a marker for transient destabilization of the plasma membrane. One major advantage of PI over TB is that it only emits fluorescence when it is intercalated in double stranded nucleic acids. Extracellular binding to the cellular membrane will, in this case, not cause fluorescence. We only evaluated the influence of the free polycations in this case to exclude piggybacking of PI on the polyplex DNA, taking into account that free polycations are anyway present in excess during transfections. Results are summarized in Figure 3.

The number of fluorescent cells and the MFI were lowest for the negative controls, and the MFI of the l-PEI-treated cells was similar to that of the negative controls throughout the experiment. Initially, a fraction of PI-positive cells was significantly higher for the l-PEI-treated cells compared to the controls, but as soon as the PI was removed from the surrounding during media exchange, the percentage of fluorescent cells decreased and 24 h after medium exchange, only ca. 20% of the l-PEI-treated cells was still PI-positive compared to 10% of the negative controls.

In the case of the Nanostar-treated cells, more than 90% of the nonapoptotic cells showed fluorescence with an MFI clearly above than of the negative controls and the l-PEI treated cells, while still being lower than the PI fluorescence typically detected for dead cells (MFI $\geq 5 \times 10^4$ au; Figure 1). Moreover, the number of fluorescent cells and their MFI stayed almost constant throughout the experiment. This is thus similar to the behavior observed with TB and corroborates the hypothesis that the Nanostar induces a transient destabilization of the plasma membrane or a reversible formation of nanopores, which allows an uptake of small normally membrane impermeant molecules. Moreover, the fact that the cells were still highly viable suggests that any permeabilization taking place was sufficiently transient and reversible to avoid permanent damage to the cells.

By comparison, any membrane permeabilization induced by l-PEI is negligible and in the range of the negative controls in terms of facilitating the passage of membrane impermeant molecules. A beneficial effect on DNA uptake is rather unlikely in this situation.

Porosity Assay in the Tube Transfection Procedure. In the past, we demonstrated that by changing the transfection settings from a plate to a microtube format, thereby increasing the cell density and reducing the polymer concentration as well as the incubation time in the transfection medium, we were able to considerably improve the transfection outcomes in the case of Jurkat cells.[12] To assess whether the improved results in

https://dx.doi.org/10.1021/acsomega.0c03367
ACS Omega 2020, 5, 26640−26654

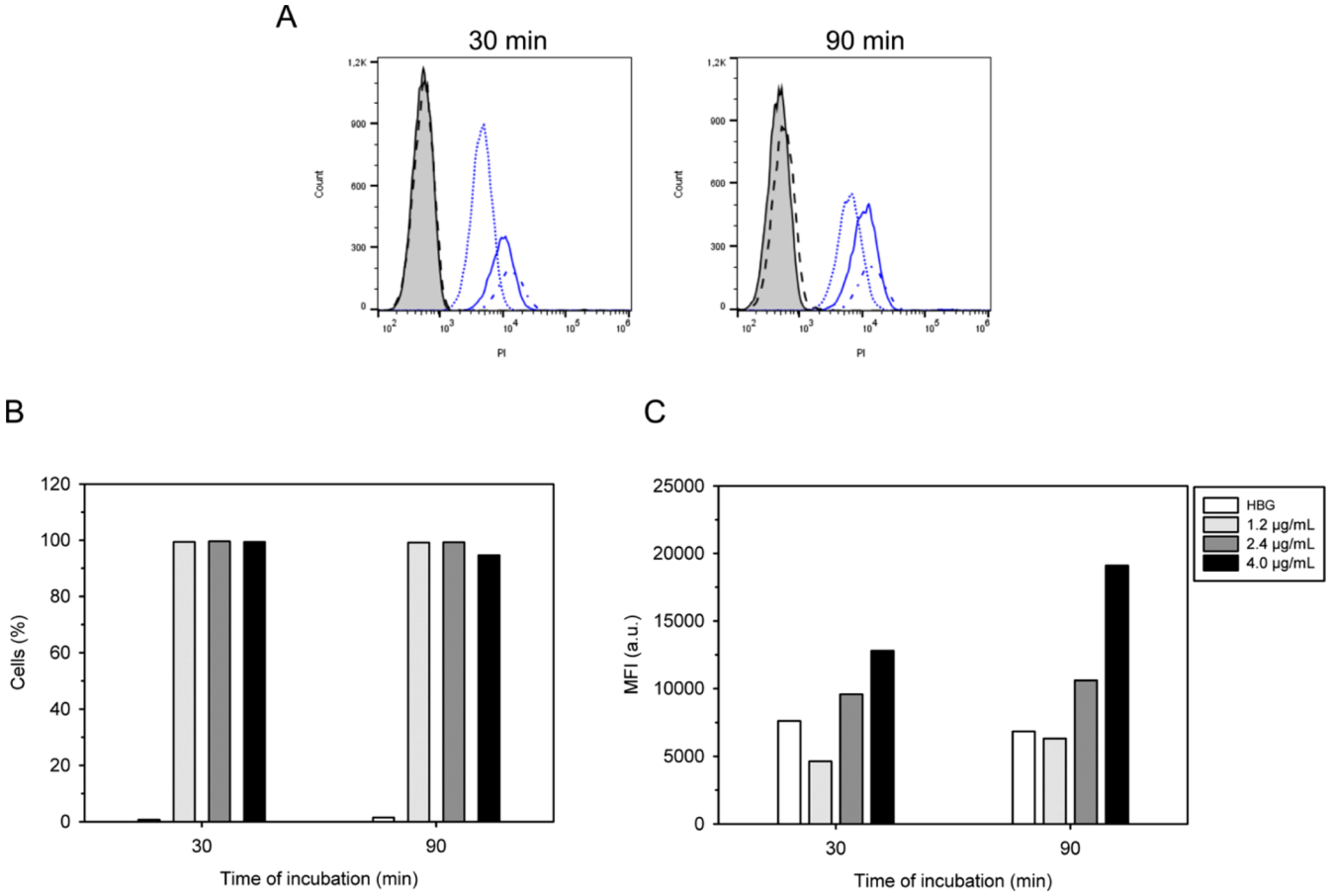

Figure 5. Cellular uptake of PI by Jurkat cells during transfection in microtubes. Cells (4×10^5 cells mL^{-1}) were incubated for 30 to 90 min in microtubes (total incubation volume: 0.5 mL; Opti-MEM (serum-free conditions)) with free polymers (Nanostar) at the indicated polymer concentrations in the presence of 1 μg mL^{-1} PI. Cells incubated with HBG served as a negative control. Representative overlays of PI fluorescence (A). Grey, control cells (incubated without PI); black dashed line, HBG; blue dotted lines, 1.2 μg mL^{-1}; blue solid lines, 2.4 μg mL^{-1}; blue dashed-dotted lines, 4.0 μg mL^{-1}. Flow cytometry results were expressed either as percentages of cells positive for PI-fluorescence in the FSC/SSC nonapoptotic gate (B) or median fluorescence for PI-positive gated cells (C). Data points represent one experiment performed in duplicates.

the microtubes were related to a similar change in the permeabilization of the cellular membrane, we reconducted transfections in microtubes in the presence of 0.001% TB. The effect of the Nanostar at concentrations and incubation times that had previously given the best transfection results was tested. The cells were transfected using 3, 6, and 10 μg polymer per 10^6 cells (1.2, 2.4, and 4.0 μg polymer mL^{-1}), and TB uptake was analyzed by flow cytometry after 30 and 90 min incubation. Previously, such experimental conditions had reproducibly led to up to 80% transfection efficiency, while transfection efficiencies of l-PEI (about 2 μg mL^{-1}) never exceed the single digit range.[12]

The results summarized in Figure 4 show that for all PPs, the percentage of TB-positive living cells was maximal after 30 min incubation followed by a statistically significant decrease after 90 min. A similar trend, albeit not statistically significant, was also detected for the free polymers at polymer concentrations $\leq$4 μg mL^{-1}. The number of TB-positive living cells was significantly higher in the polymer-treated group than in the negative control, except for the lowest polymer concentration tested, suggesting an uptake of TB as a free molecule and/or via polymer/PP piggybacking in these cases. In terms of the MFI, these values were only clearly different from the negative controls for the highest tested polymer concentration and after incubation with the free Nanostar polymer. Again, the presented results cannot fully exclude that the detected fluorescence is linked to interaction of TB with the Nanostar itself.

When the cells were incubated with free Nanostars in the presence of PI (Figure 5), almost 100% took up PI independently of the polymer concentration, whereas the controls tested negative for PI fluorescence (PI^+-cells <5%). As observed for TB, MFIs increased when the polymer concentration was raised, indicating that the amount of PI taken up by the cells is correlated to the polymer concentration. Moreover, MFIs slightly increased over time and, except for the lowest Nanostar concentration, were higher than that of the controls (i.e., "HBG").

While comparing both transfection procedures (six-well vs microtube), differences became clearly perceptible in terms of fluorescence intensity, that is, the amount of dye bound/taken up by the cells. MFIs for TB- and PI-fluorescence were always significantly higher for cells transfected in microtubes. Thus, we can hypothesize that improving the cell/polyplex contact leads to a higher permeation of the plasma membrane, which supports the assumption of an improved uptake of PPs and, in the end, a better transfection outcome. Moreover, in the microtubes, the contact time was reduced from 4 h to 30 min allowing for a better recovery of the cells (i.e., membrane

https://dx.doi.org/10.1021/acsomega.0c03367
ACS Omega 2020, 5, 26640−26654

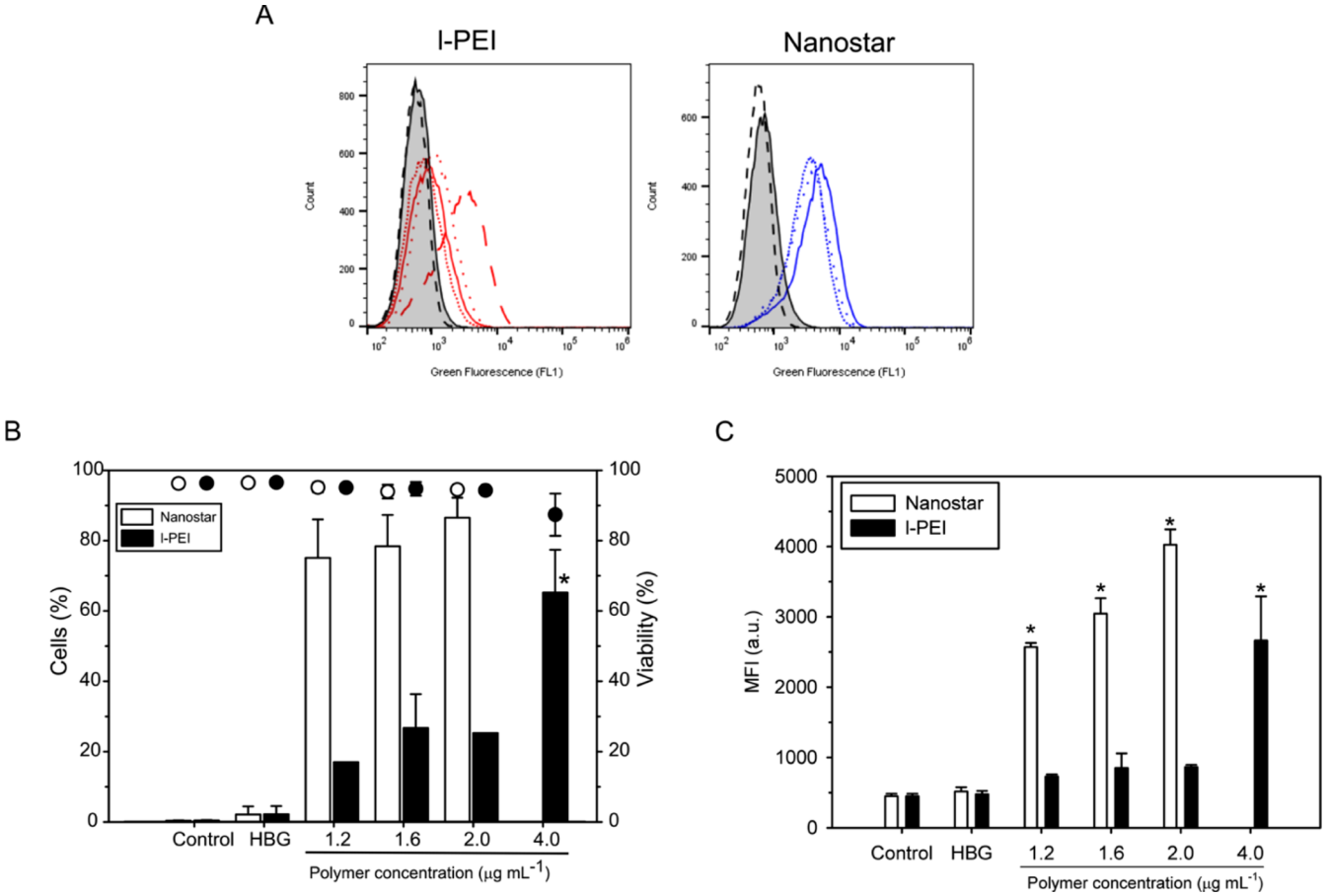

Figure 6. Cellular uptake of PS beads by the Jurkat cells during incubation with l-PEI or Nanostar-based PPs. Uptake of PS beads (100 nm) during transfection in tubes with Nanostars at N/P 10 and l-PEI at N/P 20. PPs were built in HBG with the indicated amount of polycations (final concentration during transfection). The cells (0.2×10^6 cells per microtube) were incubated for 90 min with the PPs and fluorescent-labeled plain PS beads (2×10^9 beads/microtube; 10^4 beads/cell). As controls, cells were only incubated with beads in the complexation matrix ("HBG") or just with the complexation matrix ("control"). (A) Representative overlay of the beads measured fluorescence. Grey, control cells; red, l-PEI; blue, Nanostar. Dashed line, HBG; dotted lines, 1.2 μg mL^{-1} polymer; dotted-dashed lines, 1.6 μg mL^{-1} polymer; solid lines, 2.0 μg mL^{-1} polymer; long-dashed lines, 4.0 μg mL^{-1} l-PEI. (B) Bars represent the percentage cells that have taken up the particles in the nonapoptotic cell population (FSC/SCC gate). Circles represent cell viabilities in the total population. (C) MFI. Data represent mean ± SD, $n \geq 3$ except for PEI (1.2 and 2.0 μg mL^{-1}), where $n = 1$; in that case, data represent the averaged values of one experiment carried in duplicates. *: statistically significance within a group, $p < 0.05$.

regeneration), which in turn also improves the transgene expression.

Uptake of Fluorescent Nanobeads under Conditions of Transfection. To further confirm the pore formation/permeabilization during Nanostar transfection and for a first estimate of the size of the formed holes, additional permeation studies were performed using PS beads with a diameter of 100 nm, that is, in the range of the hydrodynamic radii expected for the PPs (l-PEI: ~130 nm and[56] Nanostar: ~70.4 nm[12]). The chosen beads contained an encapsulated fluorophore and had no special functional groups on the surface. Hence, their uptake should not be biased by surface coatings or the presence of interactive dye molecules.

Cells were incubated for 90 min with Nanostars and l-PEI-based PPs in the presence of 10^4 beads per cell prior to analysis by flow cytometry. Cells incubated with an equal number of beads in the absence of PPs served as negative controls. As shown in Figure 6, the negative controls showed nothing beyond the cellular autofluorescence; that is, the Jurkat cells did not spontaneously take up the PS beads (≤2.2% fluorescent cells among the controls). In the presence of Nanostar-based PPs, 80% of the cells were fluorescent indicating that beads had been taken up. Moreover, the MFI tended to be significantly higher than that for the negative controls. Increasing the polymer concentration did not lead to a statistically significant increase of the number of fluorescent cells but to a significant further increase of the MFI. For l-PEI-based PPs built at polymer concentrations ≤2 μg mL^{-1}, the percentage of fluorescent cells never exceeded 30%, with MFIs in the range of the negative controls. Only for the highest investigated l-PEI concentration, 4 μg mL^{-1}, that is, a value already approaching the LD_{50} of l-PEI, was a doubling of the number of fluorescent cells achieved together with an MFI comparable to the effect of 1.2 and 1.6 μg mL^{-1} Nanostars. In all cases, the cell viability, detected postincubation with the cell nonpermeant dye 7-amino-actinomycin D (7-AAD), was always above 80%, indicating that uptake of the beads was not lethal to the cells.

Bead uptake, presumably by passive diffusion, is thus highly facilitated in the presence of Nanostars. Furthermore, for Nanostars, the polymer concentration during incubation seems

https://dx.doi.org/10.1021/acsomega.0c03367
ACS Omega 2020, 5, 26640−26654

to exert a distinct effect on the amounts of up taken polymer beads.

For both Nanostars and l-PEI, when beads were coincubated with PPs built at N/P 1, the number of fluorescent cells was comparable to the controls, indicating that an excess of polymer (i.e., an N/P > 1) is necessary to induce cellular uptake of the beads (Table 2). When the uptake of PS beads was investigated in the presence of PPs built at N/P 1 and an excess of the respective other polycation (free l-PEI in case of $PP_{Nanostar}$ and free Nanostars in case of PP_{PEI}) added prior to the 90 min incubation period, a significant improvement of the bead uptake was observed in all cases. However, adding an excess of Nanostar to l-PEI PPs built at N/P 1 did not induce bead uptake to the same level as observed for Nanostar PPs built at N/P 10. This suggests that the porosity induced by the Nanostar is not entirely related to the free portion of the polymer. This would be in line with recent results showing that a variability in tightness (i.e., complexation/decomplexation) and size of the PPs also influence the transfection kinetics from the cellular uptake to pDNA release ultimately determining their transfection efficiencies.[15]

Table 2. Cellular Uptake of PS Beads after Challenging with Mixed Polycation Combinations[a]

	cells (%)[c]	MFI (au)	viability (%)
$PP_{Nanostar}$ N/P1	0.9 ± 0.3	444 ± 55	95.8 ± 2.8
$PP_{Nanostar}$ N/P1 + l-PEI[b]	67.2 ± 6.2	2341 ± 451	81.0 ± 10.5
l-PEI[b]	79.8 ± 5.7	2795 ± 504	88.4 ± 7.8
PP_{PEI} N/P1	0.6 ± 0.2	404 ± 25	96.7 ± 0.5
PP_{PEI} N/P1 + Nanostar[b]	25.3 ± 2.0	923 ± 118	92.8 ± 1.1
Nanostar[b]	85.1 ± 9.9	3174 ± 350	92.3 ± 2.8

[a]The PPs were built with 1.6 μg mL^{-1} polymers adjusting the N/P ratio to 1 by adding a suitable amount of pDNA (Nanostar: 14.7 μg mL^{-1} pDNA; l-PEI: 54.4 μg mL^{-1} pDNA). MFI: median fluorescence intensity. [b]"l-PEI" and "Nanostar" correspond to the respective amount of free polymer added to the PP at N/P 1 (i.e., for $PP_{Nanostar}$: 4 μg mL^{-1} free l-PEI; for PP_{PEI}: 1.6 μg mL^{-1} free Nanostar). [c]The Percentage of green cells containing PS beads. PP: polyplexes. Data represent mean ± SD, n = 2.

Uptake of Fluorescently Labeled PPs by Isolated Nuclei. One major hurdle in the transfection of nondividing or slow growing cells is the crossing of the nuclear membrane. Since the Nanostar is capable of transiently disrupting the plasma membrane, it was of interest to determine whether this polycation can deliver pDNA to the nucleus via direct permeabilization of the nuclear membrane. PPs (r_h: 100−200 nm) and pDNA molecules of a typical size (4−12 kbp, r_h supercoiled molecule: 10−20 nm)[57] are too large to autonomously pass this membrane. In contrast to the plasma membrane, the nuclear envelope contains open pores, which allow the crossing of small molecules (≤40 kDa, cutoff 5 nm). Taking this into account, the settings used previously to assess plasma membrane porosity using small charged dye molecules were not appropriate in a study of the permeabilization of the nuclear membrane. Instead an approach using labeled pDNA to build labeled PPs was chosen.

pDNA can be labeled with fluorescent dyes, which bind/intercalate firmly into the double helix in a stoichiometric manner.[53] However, during polyplex formation, the compaction of the pDNA is known to lead to dye exclusion depending on the condensation capacity of the polymer.[58] Therefore, we first evaluate the stability of the pDNA stain in PPs. pDNA was preloaded with three standard dyes for nucleic acids (i.e., PI, 7-AAD, and SyBRGreen (SB)),[59−61] and the residual fluorescence was measured after complexation with l-PEI and the Nanostar. The final dye concentration was set at 1 μg mL^{-1} as previously described by Schacht and co-workers.[62]

The above presented results at the cellular level showed that an excess of polycation (i.e., N/P > 1) was necessary to induce membrane permeabilization. However, within the intracellular environment, the original excess of polycations will be neutralized by intracellular polyanions and PPs reaching the nuclei will likely have a N/P ratio close to 1. Therefore, we restricted our testing to PPs built at an N/P of 1. The fluorescence of the l-PEI PPs was high in all cases, Table 3. Due to the stoichiometric binding of the dyes, the emitted fluorescence is proportional to the amount of pDNA. Since a 10-fold lower amount of pDNA was used to produce the PPs, a somewhat lower fluorescence was expected for the Nanostar PP. In the end, the detected fluorescence was about 5-fold lower. Whereas pDNA preloaded with SG and PI displayed weak to no fluorescence after complexation with the Nanostar, the fluorescence signal from Nanostar PPs containing 7-AAD-stained pDNA should be sufficiently high and stable (Nanostar PP built with 5 μg of polymer) to analyze the uptake of the corresponding PPs into the nuclei by flow cytometry.

For the experiment, purified nuclei were incubated with the respective PPs (N/P 1, 5 μg polymer per assay) built with 7-AAD preloaded pDNA. The 7-AAD concentration (i.e., 1 μg mL^{-1}) applied in these experiments is 10-fold lower than the standard concentration used for specific DNA detection during cell cycle analysis[63] and hence was expected to keep the fluorescence due to spontaneous diffusion of 7-AAD through the NPCs, low. After 30 min incubation at 37 °C, the fluorescence of the nuclei was analyzed by flow cytometry.

Table 3. Overview of Fluorescence of pDNA Pre-loaded with Nucleic Acid Dyes in PPs[a]

	fluorescence (au)			
	l-PEI		Nanostar	
	5 μg per assay	2.5 μg per assay	5 μg per assay	2.5 μg per assay
PI	42,304 ± 594	19,728 ± 224	b.d.	b.d.
SG	41,433 ± 987	21,869 ± 452	2982 ± 26	590 ± 18
7-AAD	38,196 ± 1592	17,281 ± 288	6626 ± 82	1418 ± 224

[a]PP were prepared in a final volume of 50 μL of HBG by mixing suitable amounts of preloaded pDNA with 2.5 or 5 μg of polymer to reach a N/P ratio of 1. Polymer concentrations tested are in the range of the ones used for PP formation in standard transfection protocols prior to dilution with Opti-MEM. Fluorescence of SG was measured at Ex: 485 ± 20 nm/Em: 535 ± 20 nm. Fluorescence of PI and 7-ADD was measured at Ex: 535 ± 20 nm/Em: 670 ± 20 nm. The values represent ($F_{sample} - F_{blank}$) with $F_{blank,PI}$: 3786 ± 251; $F_{blank,SG}$: 64 ± 16; $F_{blank,7\text{-}AAD}$: 6450 ± 129. Data represent mean ± SD, n = 3. b.d.: below detection limit.

https://dx.doi.org/10.1021/acsomega.0c03367
ACS Omega 2020, 5, 26640−26654

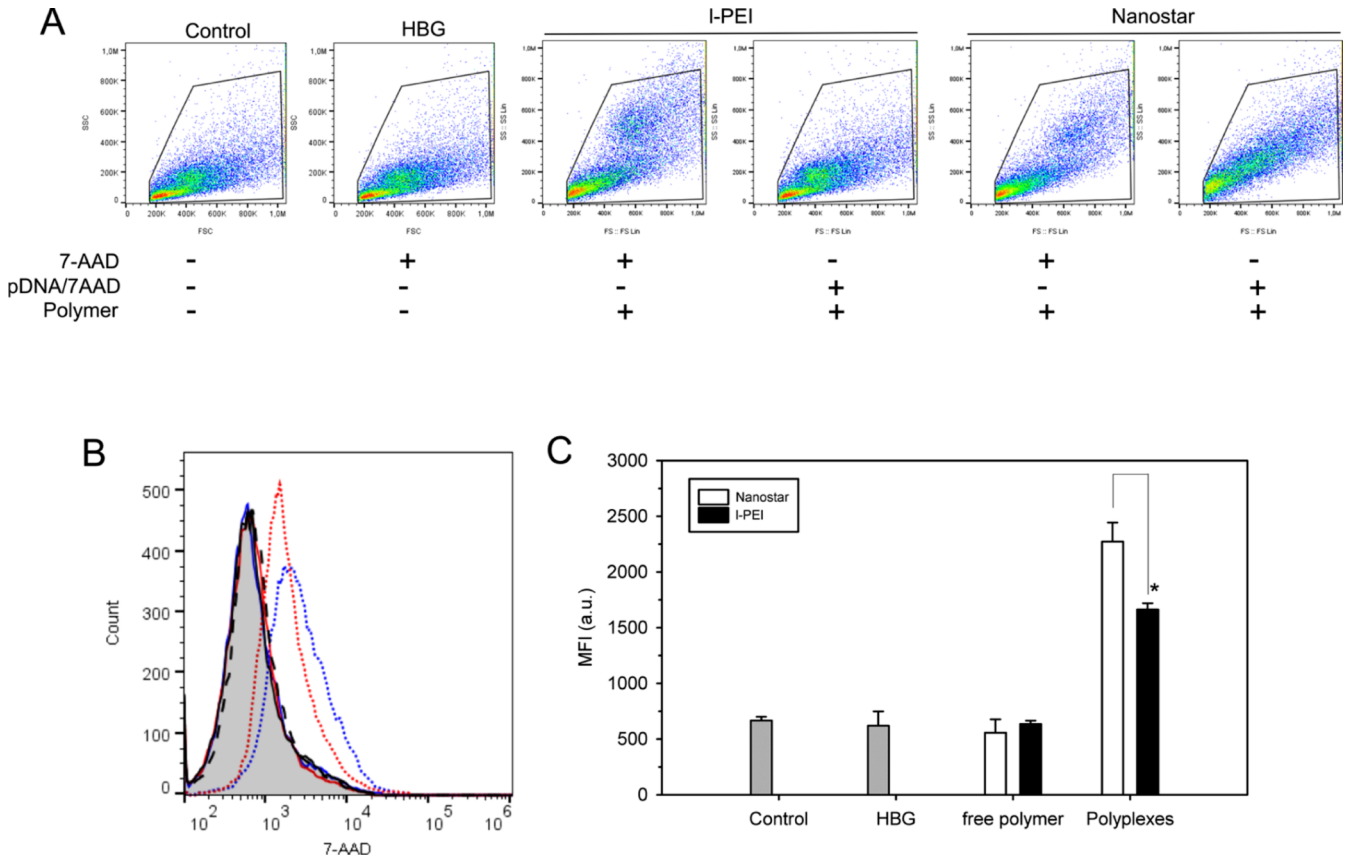

Figure 7. Uptake of PPs in isolated nuclei. 5×10^5 nuclei isolated from Jurkat cells were incubated with free polymers or PPs (10 μg polymer mL^{-1}) prepared at N/P 1 with pDNA prelabeled with 7-AAD (pDNA/7-AAD). Total incubation volume of 500 μL. After 30 min incubation at 37 °C, nuclei were analyzed by flow cytometry. (A) Representative scatter plots of the nuclei. Control: nuclei mock-incubated without 7-AAD; HBG: nuclei mock-incubated with 1 μg mL^{-1} unbound 7-AAD. (B) Representative overlay of the 7-AAD measured fluorescence. Grey, control nuclei; red, l-PEI; blue, Nanostar. Dashed line, HBG; solid lines, free polymers; dotted lines, PPs. (C) MFI of 7-AAD. Free polymer: nuclei incubated with free polymers and with 1 μg mL^{-1} unbound 7-AAD; PPs: nuclei incubated with PPs built with 7-AAD-pre-loaded pDNA. Data represent mean ± SD, $n = 2$. Statistical significance (ANOVA, $p < 0.05$) is indicated by *.

Nuclei incubated with 7-AAD only and with free polymers plus 7-AAD were used as controls to evaluate the fluorescence intensity after spontaneous uptake of 7-AAD with and without free polycations, Figure 7. The fluorescence of nuclei incubated with 7-AAD with or without free polymers was similar to the nontreated nuclei. This indicates that the concentration of 7-AAD used in this assay was not high enough to lead to a detectable increase of the nuclei fluorescence.

In the presence of 7-AAD-pre-loaded pDNA, the fluorescence of nuclei incubated with both types of PPs was higher than the fluorescence of nuclei incubated with free polymers. However, the shift toward higher fluorescence was more pronounced for $PP_{Nanostar}$ than for PP_{PEI}. Considering that the fluorescence of $PP_{Nanostar}$, as measured in plate reader assay (Table 3), was about 5-fold lower than that of PP_{PEI}, the difference in the amount of PPs actually reaching the nucleus was even more pronounced than indicated by the differences in the fluorescence intensity.

Apparently both types of PPs are able to transfer the labeled DNA into the nucleus when present in close proximity to the nuclear membrane, while the effect is more pronounced for Nanostars. In a recent contribution, Silva's group identified the nuclear entry as a bottleneck for linear PDMAEMA-driven gene delivery in postmitotic (i.e., nondividing) cells.[17] Our results suggest that the PDMAEMA-based Nanostars can transfer DNA into the nucleus; therefore, we can hypothesize that the architecture of the polymer more than its chemistry plays a major role for the passage of the nuclear envelope. Recently, the nuclear uptake of the bPEI-based PP using the DNA-intercalating dye YOYO-1 in HepG2 cells showed that after 4 h incubation in serum-free medium, bPEI-25 kDa/pDNA PPs delivered only 30.9% of the pDNA into the nucleus as detected by flow cytometry of isolated nuclei.[15] A principle limitation of the use of flow cytometry for the uptake studies is the inability of the methods to distinguish between fluorescent materials truly inside the nucleus and those merely attached to the nuclear membrane. Nevertheless, there is evidence that Nanostars are more efficient than l-PEI in allowing the uptake of their cargo into the nucleus presumably due to membrane destabilization as previously observed at the level of cellular uptake (Figures 2–6). Therefore, we hypothesize that the significantly higher gene transfection efficiency achieved with the Nanostar can partly be ascribed to an enhanced nuclear membrane permeability improving plasmid accumulation in the nucleus. Additional studies will be necessary to fully decipher the nuclear uptake mechanisms of PEI- and Nanostar-based PPs.

CONCLUSIONS

Elucidating the bottlenecks of plasmid mass transfer during transfection can enable an improved understanding of structure–function relationships in the polymeric materials,

https://dx.doi.org/10.1021/acsomega.0c03367
ACS Omega 2020, 5, 26640–26654

thereby leading to the next generation of rationally designed nonviral gene delivery vectors. This study aimed at evaluating the permeation capability of the star-shaped delivery vector (Nanostar) developed by our group over the last decade in comparison to l-PEI, which is still the gold standard for polycationic gene transfection. These two polycations vary in their chemistry, architecture, and molecular weight. A flow cytometry-based method was developed to evaluate the permeabilization of the cellular and nuclear membrane after transfection. From our results, only the Nanostar-based PPs effectively transport the pDNA into the nucleus via reversible destabilization of the plasma membrane, most likely through transient pores formation. This might be an explanation for the efficient gene delivery capability of Nanostars in cells that are notoriously difficult to transfect.

Moreover, Nanostars and, to a lesser extent, l-PEI increased the nuclear membrane association/permeability allowing accumulation of structures larger than the NPC on/in the nucleus. Further studies of the mechanism of nuclear uptake are the focus of the ongoing studies in our group. Since the Nanostar is able to permeabilize biological membranes, they might also permeabilize the membrane of different organelles including endosomal structures. Further study on polyplex interactions with other organelles could be of high interest since PPs are present within the cells for an extended time period after the removal of the transfection mixture and could potentially interact with many intracellular processes. In the future, it might become possible to tailor polymers that specifically permeabilize the nuclear envelope to increase pDNA delivery to the nucleus but do not extensively damage the nuclei to avoid cells committing apoptosis.

MATERIALS AND METHODS

Materials. If not otherwise indicated, we used Greiner Bio-One (Frickenhausen, Germany) as the supplier for cell culture materials and Sigma-Aldrich (Taufkirchen, Germany) for chemicals. 2-(*N*,*N*-Dimethylamino)ethyl methacrylate (DMAEMA, 98%) was passed through a basic alumina column prior to polymerization. Anisole (>99%), copper(I) bromide (CuBr, 99.999%), copper(II) bromide ($CuBr_2$, 99%), dimethyl sulfoxide, ethyl 2-bromoisobutyrate (EBiB), 1,1,4,7,10,10-hexamethyltriethylenetetramine (HMTETA, 98%), and 1,3,5-trioxane (>99%) were used without further purification. Linear PEI (l-PEI, 25 kDa) was from Polysciences (Polysciences Europe GmbH, Eppenheim, Germany). Fetal calf serum (FCS) was from Biochrom (Biochrom AG, Berlin, Germany). Dulbecco's phosphate-buffered saline (DPBS) without Ca^{2+} and Mg^{2+} was from Lonza (Visp, Switzerland). HBG buffer (20 mM Hepes, 5 wt % glucose, pH 5.5) was prepared in house and sterilized by filtration. Cell culture media R10 (RPMI 1640 without glutamine, with 10 vol % FCS, 2 mM L-glutamine, 100 IU/mL penicillin, and 100 μg mL^{-1} streptomycin) and Opti-MEM with GlutaMAX were from Biochrom and Thermo Fisher Scientific (Dreieich, Germany), respectively. For pre-equilibration, media were incubated for 1 to 4 h in a standard mammalian cell culture incubator (37 °C, 5% CO_2, 95% humidity). TB solution (0.4%) was from VWR (VWR International, Ismaning, Germany). PI, 7-AAD, and SyBRGreen I (SG) were from Sigma-Aldrich. PS beads (micromer-greenF plain particles, green fluorescent, 100 nm) were from micromod Partikeltechnologie GmbH (Rostock, Germany) and supplied as a generous gift from Prof. Feldhaar, University of Bayreuth, within the collaborative framework of CRC 1357. Plasmid pEGFP-N1 (4.7 kb) used for polyplex formation was from Clontech Laboratories, Inc. (Mountain View, CA). The plasmid was amplified in *Escherichia coli* (LB medium) using standard laboratory techniques. The EndoFree Plasmid Kit (Giga Prep/Maxi Prep) from QIAGEN (Hilden, Germany) was used for purification (quality control: >80% supercoiled topology (agarose gel) and $A_{260}/A_{280} \geq 1.8$). Purified plasmids were solubilized in sterile PCR water (Sigma-Aldrich).

Synthesis and Characterization of the PDMAEMA Nanostar. Atom-transfer radical polymerization (ATRP) was performed in a grafting-from approach with bromo-isobutyrate-functionalized silsesquioxane (24-arm stars) as the initiator. The synthetic procedures have been previously published.[11,64] Briefly, for the star-shaped polymers, DMAEMA, CuBr, $CuBr_2$, trioxane, and anisole (flask 1), as well as the respective initiator, HMTETA, and anisole (flask 2) were weighed into sealable flasks and separately degassed with nitrogen for 15 min. The initiator solution (flask 2) was then transferred with the help of a syringe and minimal contact to air to the monomer solution (flask 1). The polymerization was started by stirring the reaction mixture in a thermostated oil bath at 60 °C. For the determination of the conversion, the disappearance of the vinyl signals compared to the trioxane signal as a control was monitored by ^{1}H NMR spectroscopy. At appropriate conversion, samples were withdrawn from the reaction mixture under a nitrogen atmosphere, then opened to air, diluted with dioxane, and dialyzed against a mixture of dioxane and Milli-Q water for purification. The pure polymers were obtained as white powders after freeze-drying. Ion-coupled plasma−mass spectrometry showed <150 mg/kg copper remaining in the dried powder after dialysis. Arm numbers of the Nanostars were determined using a published procedure.[65]

Nuclear Magnetic Resonance Spectroscopy. To monitor the conversion of the DMAEMA polymerizations, NMR spectra were recorded on a Bruker AVANCE (Ultrashield) 300 instrument (300 MHz) in deuterated chloroform (Deutero GmBH, Kastellaun, Germany) as the solvent. The signal of $CHCl_3$ was used for calibration (7.26 ppm for ^{1}H).

Size Exclusion Chromatography. The apparent molecular weights and their distributions of the PDMAEMA samples after dissolving them overnight were determined using dimethylformamide as the eluent. The equipment consisted of one precolumn and two analytical columns (PSS GRAM, 102 and 103 Å pore size, 7 mm particle size) and a refractive index detector. The measurements were performed at 60 °C, and linear poly(methyl methacrylate) standards with a narrow molecular weight distribution and methyl benzoate as the internal standard were used for calibration.

Polycationic Transfection Agents. Transfection agents were l-PEI (25 kDa) and a well-defined 24-armed star (referred to as Nanostar) synthesized via ATRP of DMAEMA. An average Nanostar consists of an inorganic core decorated with polycationic PDMAEMA arms, each with an average length of 230 monomeric units. The number average molecular weight, M_n, of the construct was 755 kDa, and the polydispersity was (M_w/M_n) < 1.21. Polymer stock solutions were prepared in sterile ultrapure PCR-water (Sigma-Aldrich) as 1.25 mg mL^{-1} (l-PEI) and 1.82 mg mL^{-1} (Nanostar) and diluted for use as indicated. LD_{50} values were 12.1 μg mL^{-1} for l-PEI[66] and 500 μg mL^{-1} for Nanostar[11] as determined by MTT assay.

https://dx.doi.org/10.1021/acsomega.0c03367
ACS Omega 2020, 5, 26640−26654

Cell Line and Maintenance. Jurkat cells (TIB-152, ATCC) were maintained in R10, as suggested by the supplier. A seeding density of 1×10^5 cells mL^{-1} was used during passaging and the maximal cell density was never allowed to exceed 3×10^6 cells mL^{-1}. Cells were cultivated at 37 °C in a humidified 5% CO_2 atmosphere. Cell numbers and viabilities during passaging and seeding steps were evaluated by TB exclusion assay with a hemocytometer (Neubauer Improved, VWR International, Ismaning, Germany) according to standard laboratory protocols.

Nuclei Isolation. For the isolation of nuclei, exponentially growing Jurkat cells were collected by centrifugation (5 min, 200*g*) and rinsed once with ice-cold DPBS and once with ice-cold buffer A (10 mM Tris pH 7.4−10 mM NaCl—3 mM $MgCl_2$—1 mM DTT). The cells were then incubated in buffer A for 30 min on ice to allow for swelling. Afterward, the cell suspension was transferred into a precooled Dounce homogenizer ("loose" pestle B with a clearance of about 0.7 mm, VWR International GmbH, Darmstadt, Germany), and the cellular membrane was disrupted by 47 strokes. The lysed cells were loaded on the top of an ice-cold sucrose cushion (10 mM Tris pH 7.4−10 mM NaCl—3 mM $MgCl_2$—7.5 mM DTT—30% (w/v) sucrose) and centrifuged at 4 °C, 800*g* for 20 min. This step was repeated twice to remove nonlysed cells. The pellet containing the nuclei was mechanically dislocated, and the nuclei were washed once with ice-cold DPBS and then with ice-cold Opti-MEM (5 min, 400*g*, 4 °C) to wash out any residual chemicals of the nuclei preparation. The nuclei pellet was resuspended in ice-cold Opti-MEM. Nuclei were counted with a hemocytometer, and the nuclei density was set at 1×10^7 nuclei mL^{-1}. Nuclei were stored on ice until use.

TB Exclusion Assay by Flow Cytometry. The fluorescence emitted by living and dead cells stained with various concentrations of TB was evaluated by flow cytometry. Exponentially growing cells (viability >90%) were harvested by centrifugation and washed twice with DPBS. Then, the cell density was set to 1.0×10^6 living cells mL^{-1} in Opti-MEM. An aliquot of this cell suspension was incubated at 50 °C for 45 min to produce the "dead cell" population. 10^5 living cells in 100 μL of Opti-MEM were then mixed with 100 μL of 0.002 to 0.4% TB solutions in Opti-MEM. The cells were incubated for 5 min on ice prior to flow cytometry analysis. Cells stained with 1 $\mu g\ mL^{-1}$ PI were used for comparison.

Analysis of PP Fluorescence after Incubation with TB and PI. Fluorescence related to the interaction of TB and PI with free polymers and PPs as well as the intercalation of PI into complexed DNA was analyzed using a plate reader (Genios Pro, Tecan, Crailsheim, Germany). Each experiment was performed in duplicates. Noncomplexed pDNA was prepared as the control. PPs were prepared in a final volume of 200 μL by first diluting the necessary volume of pDNA stock solution (1.0 mg mL^{-1}) in HBG followed by the addition of 5 to 10 μg of polymer per tube for l-PEI and the Nanostar, respectively, to reach N/P ratios (polymer N to DNA P) of 10 (Nanostar) and 20 (l-PEI). In the previous studies, we have investigated the physicochemical properties of these PPs and established the indicated N/P ratios as optimal for transfection with these polymers.[11,12,56,66] The mixture was vortexed for 10 s and incubated for 20 min at room temperature. Then, one volume of a 0.002% TB solution or a 2 $\mu g\ mL^{-1}$ PI solution was added. After mixing, 200 μL of the mixture was transferred into a flat-bottom black 96-well plate, and the fluorescence was measured in the plate reader. The following filter pairs Ex: 485 nm/Em: 670 nm and Ex: 535 nm/Em: 612 nm were used to measure TB and PI fluorescence, respectively.

Polyplex Formation with Fluorescently Labeled pDNA. pDNA was preloaded with various nucleic acid stains (PI, SG, and 7-AAD) by adding suitable volumes of nucleic acid stain stock solutions (PI and 7-AAD: 100 $\mu g\ mL^{-1}$; SG: 100×) to the pDNA solution to reach final concentrations of 1 $\mu g\ mL^{-1}$ (PI, 7-AAD) and 1× for SG. The mixture was then incubated for 20 min at room temperature in the dark. PP were prepared in a final volume of 50 μL by first diluting the necessary volume of the preloaded pDNA stock solution (1.7 mg mL^{-1}) in HBG followed by the addition of 2.5 (l-PEI) or 5 μg of (Nanostar) polymer per tube to reach a N/P ratio of 1. The mixture was vortexed for 10 s and incubated for 20 min at room temperature. Then, the mixtures were transferred into a flat-bottom black 96-well plate, and the fluorescence of the intercalated dyes was measured by a plate reader using the following filter pairs: Ex.: 485 ± 20 nm/Em: 535 ± 20 nm for SG, Ex: 535 ± 20 nm/Em: 670 ± 20 nm for PI and 7-AAD. Noncomplexed preloaded pDNA was used as the control.

Porosity Testing with Cell Impermeant Dyes. Membrane permeabilization was analyzed via the cellular uptake of the membrane impermeable dyes TB (0.001%) and PI (1 $\mu g\ mL^{-1}$) during the course of the transfection. Cells and PPs were prepared as described previously,[12] and TB or PI was supplemented into the transfection mixture prior to the addition to the cells. Briefly, cells were harvested by centrifuging 24 h before transfection and seeded at 0.05×10^6 living cells mL^{-1} in R10. On the day of the experiment, the exponentially growing cells (viability > 90%) were harvested by centrifugation, washed twice with DPBS, and seeded at 0.2×10^6 living cells mL^{-1} in six-well plates or 2 mL Eppendorf tubes (referred to as microtubes) in 1 mL of pre-equilibrated (60 min incubation in the cell culture incubator) Opti-MEM. The plates were put back into the incubator, while the microtubes were stored on ice for 1 h. In the meantime, PPs were prepared in final volumes of 50 (microtubes) and 200 μL (6-well plates) by first diluting a suitable amount of pDNA stock solution (1 mg mL^{-1}) in HBG, followed by the addition, in a single drop, of the polymer stock solution (Nanostar: N/P 10, 50 μg polymer per 10^6 cells, 4.5 $\mu g\ mL^{-1}$; l-PEI: N/P 20, 25 μg polymer per 10^6 cells, and 2.3 $\mu g\ mL^{-1}$). The mixture was immediately vortexed for 10 s and incubated for 20 min at room temperature. Then, 1 mL (6-well plates) or 0.45 mL (microtubes) of pre-equilibrated Opti-MEM was added, followed by another 10 min incubation at room temperature.

In case of the six-well plates, the PPs or the free polymer mixture (1.2 mL total volume) supplemented with 0.001% TB or 1 $\mu g\ mL^{-1}$ PI were added drop-wise to the 1 mL of cell suspension in the wells and distributed by gently rocking the plate. After an incubation period of up to 4 h in the cell culture incubator, the supernatant was carefully removed and replaced by 2 mL of fresh growth medium containing 10% FCS (R10). The cells were further incubated for up to 24 h. During this time, the uptake of TB and PI was regularly analyzed by flow cytometry as indicated.

In case of the microtubes, the cells stored on ice were recovered by centrifugation (200*g*, 5 min) and the supernatant was discarded. The cell pellet was mechanically dislocated prior to adding the PPs or the free polymer mixture (0.5 mL total volume) supplemented with 0.001% TB or 1 $\mu g\ mL^{-1}$ PI. After gentle mixing, the microtubes were placed upright in the

https://dx.doi.org/10.1021/acsomega.0c03367
ACS Omega 2020, 5, 26640−26654

cell culture incubator for 30 or 90 min prior to analysis by flow cytometry. In all cases, cells incubated with TB or PI in the absence of polymers/PPs served as negative controls.

To monitor the porosity of the PPs/polymers at the nuclei level, Nanostar-based PPs were prepared at N/P 1 with pDNA preloaded with 7-AAD (5 to 10 μg polymer/10^6 nuclei; 5 × 10^5 nuclei per assay). The nuclei were then challenged as described above for the cells using the microtube procedure (incubation 30 min).

Porosity Testing with PS Beads. Exponentially growing cells (viability > 90%) were harvested by centrifugation, washed twice with DPBS, seeded at 0.2 × 10^6 living cells mL^{-1} in 2 mL Eppendorf tubes, and stored on ice as described above. In the meantime, PPs were prepared in final volumes of 50 μL by first diluting a suitable amount of pDNA stock (1 mg mL^{-1}) in HBG, followed by addition, in a single drop, of the polymer stock to get N/P ratios of 10 and 20 for the Nanostar and l-PEI, respectively. Polymer concentrations from 1.2 to 4.5 μg polymer mL^{-1} were tested. In some cases, PPs were built at N/P 1 with 1.6 μg mL^{-1} polymer and 14.7 to 54.4 μg mL^{-1} pDNA for the Nanostar and l-PEI, respectively. The mixture was immediately vortexed for 10 s and incubated for 20 min at room temperature. Then, 0.45 mL of pre-equilibrated Opti-MEM was added followed by another 10 min incubation at room temperature. The cells stored on ice were recovered by centrifugation, and the supernatant was discarded. The cell pellet was mechanically dislocated prior to adding the PPs (0.5 mL total volume). After gentle mixing, 2 × 10^9 PS beads in ultrapure water (10.5 μL), corresponding to 10^4 beads per cell were added. If indicated, for PPs prepared at N/P 1, an additional 1.6 μL of PEI (1.25 mg mL^{-1}) or 4.4 μL of Nanostar (0.18 mg mL^{-1}) solution corresponding to 4 μg mL^{-1} l-PEI or 1.6 μg mL^{-1} Nanostar was added. After gentle mixing, microtubes were placed upright in the cell culture incubator for 90 min. Thereafter, cells were washed twice with DPBS and resuspended in 500 μL of DPBS prior to analysis by flow cytometry.

Flow Cytometry. For flow cytometry (Cytomics FC500 equipped with a 488 nm laser, Beckman Coulter, Krefeld, Germany), cells were recovered by centrifugation and resuspended in 500 μL of DPBS. After 2 and 4 h (6-well plate) or after 30 and 90 min (tubes), 0.001% TB or 1 μg mL^{-1} PI was added according to the cell culture standard protocol to allow differentiating vital from dead cells. FSC, SSC, and TB or PI fluorescence were recorded. Cells were initially evaluated by scatter properties (FSC/SSC) to select a region representing single, nonapoptotic cells, while disregarding dead cells, debris, and cellular aggregates. For both PI- and TB-treated cells and for the bead experiments, at least 20,000 events were acquired into the nonapoptotic living cell gate, based on size versus granularity (FSC/SSC) dot plots. Nuclei (20,000 events) were directly measured after incubation without any further centrifugation step, and FCS, SSC, and 7-AAD-fluorescence were recorded. The singlet population of nuclei was identified using FSC/SSC plots. Histogram plots of the respective fluorescence intensities (log scale) were used to estimate the percentage and the corresponding MFI of PI-positive cells (620 nm, FL3), PS bead-positive cells (525 nm, FL1), and TB-positive cells as well as 7-AAD-positive nuclei (655 nm, FL4). Cells with fluorescence intensities <10^3 au were classified as TB, PI, or bead negative living cells. Cells with fluorescence intensities between 10^3 and 3 × 10^4 au were classified as TB, PI, and bead positive living cells. Cells with fluorescence intensities >3 × 10^4 au were considered dead cells, based on previous experience with such cells. If indicated, dead cells, counterstained with PI, were evaluated in the total measured cell population. Flow cytometry data were evaluated using FlowJo software v 10.5.0 (Tree Star, Stanford University, CA, USA, 2018).

Statistical Analyses. Group data are reported as mean ± SD, with n representing the number of independent experiments. Sigma Plot software (version 11.0, Systat software Inc., San Jose, CA, USA, 2008) was used for one-way ANOVA with Bonferoni multiple comparison tests to determine whether data groups differed significantly from each other. Statistical significance was defined as $p < 0.05$.

AUTHOR INFORMATION

Corresponding Author

Ruth Freitag − *Process Biotechnology, University of Bayreuth, 95440 Bayreuth, Germany;* orcid.org/0000-0003-4642-897X; Email: ruth.freitag@uni-bayreuth.de

Authors

Valérie Jérôme − *Process Biotechnology, University of Bayreuth, 95440 Bayreuth, Germany*

Christopher V. Synatschke − *Max Planck Institute for Polymer Research, 55128 Mainz, Germany*

Complete contact information is available at: https://pubs.acs.org/10.1021/acsomega.0c03367

Notes

The authors declare no competing financial interest.

ACKNOWLEDGMENTS

This work was funded by the Upper Franconian Trust (Oberfrankenstiftung, Bayreuth, Germany) grant P-Nr.: 03847. This publication was funded by the German Research Foundation (DFG) and the University of Bayreuth in the funding program Open Access Publishing. Oberfrankenstiftung did not participate in any way in the design of this study or the collection, analysis or interpretation of the data, or in writing this article and any other decision concerning its publication. Prof. Heike Feldhaar is acknowledged for providing the PS beads within the collaborative framework of the CRC 1357—Project Number 391977956. Ariana Seira Calderon Moreno and Max Puhlmann supported this study by performing some of the transfections in six-well plates and microtubes, respectively. Andrea Schott supported this study by purifying the plasmid. The authors thank Merle Drews and Nicole Pittel for technical assistance.

REFERENCES

(1) Helal, N. A.; Osami, A.; Helmy, A.; McDonald, T.; Shaaban, L. A.; Nounou, M. I. Non-viral gene delivery systems: hurdles for bench-to-bedside transformation. *Pharmazie* **2017**, *72*, 627−693.

(2) Patil, S.; Gao, Y.-G.; Lin, X.; Li, Y.; Dang, K.; Tian, Y.; Zhang, W.-J.; Jiang, S.-F.; Qadir, A.; Qian, A.-R. The Development of Functional Non-Viral Vectors for Gene Delivery. *Int. J. Mol. Sci.* **2019**, *20*, 5491.

(3) Ni, R.; Feng, R.; Chau, Y. Synthetic Approaches for Nucleic Acid Delivery: Choosing the Right Carriers. *Life* **2019**, *9*, 59.

(4) Gigante, A.; Li, M.; Junghänel, S.; Hirschhäuser, C.; Knauer, S.; Schmuck, C. Non-viral transfection vectors: are hybrid materials the way forward? *Med. Chem. Commun.* **2019**, *10*, 1692−1718.

(5) Fischer, D.; Bieber, T.; Li, Y.; Elsässer, H. P.; Kissel, T. A novel non-viral vector for DNA delivery based on low molecular weight,

branched polyethylenimine: Effect of molecular weight on transfection efficiency and cytotoxicity. *Pharm. Res.* **1999**, *16*, 1273−1279.
(6) Godbey, W. T.; Mikos, A. G. Recent progress in gene delivery using non-viral transfer complexes. *J. Controlled Release* **2001**, *72*, 115−125.
(7) Zakeri, A.; Kouhbanani, M. A. J.; Beheshtkhoo, N.; Beigi, V.; Mousavi, S. M.; Hashemi, S. A. R.; Karimi Zade, A.; Amani, A. M.; Savardashtaki, A.; Mirzaei, E.; Jahandideh, S.; Movahedpour, A. Polyethylenimine-based nanocarriers in co-delivery of drug and gene: a developing horizon. *Nano Rev. Exp.* **2018**, *9*, 1488497.
(8) Agarwal, S.; Zhang, Y.; Maji, S.; Greiner, A. PDMAEMA based gene delivery materials. *Mater. Today* **2012**, *15*, 388−393.
(9) Tanasienko, I. V.; Yemets, A. I.; Finiuk, N. S.; Stoika, R. R.; Blume, Y. B. DMAEM-based cationic polymers as novel carriers for DNA delivery into cells. *Cell Biol. Int.* **2015**, *39*, 243−245.
(10) Li, L.; Wei, Y.; Gong, C. Polymeric Nanocarriers for Non-Viral Gene Delivery. *J. Biomed. Nanotechnol.* **2015**, *11*, 739−770.
(11) Schallon, A.; Synatschke, C. V.; Jérôme, V.; Müller, A. H. E.; Freitag, R. Nanoparticulate nonviral agent for the effective delivery of pDNA and siRNA to differentiated cells and primary human T lymphocytes. *Biomacromolecules* **2012**, *13*, 3463−3474.
(12) Riedl, S.; Kaiser, P.; Raup, A.; Synatschke, C.; Jérôme, V.; Freitag, R. Non-Viral Transfection of Human T Lymphocytes. *Processes* **2018**, *6*, 188−205.
(13) Stahlschmidt, U.; Jérôme, V.; Majewski, A.; Müller, A.; Freitag, R. Systematic Study of a Library of PDMAEMA-Based, Superparamagnetic Nano-Stars for the Transfection of CHO-K1 Cells. *Polymers* **2017**, *9*, 156.
(14) Durymanov, M.; Reineke, J. Non-viral Delivery of Nucleic Acids: Insight Into Mechanisms of Overcoming Intracellular Barriers. *Front. Pharmacol.* **2018**, *9*, 971.
(15) Kim, K.; Hwang, H. S.; Shim, M. S.; Cho, Y.-Y.; Lee, J. Y.; Lee, H. S.; Kang, H. C. Controlling complexation/decomplexation and sizes of polymer-based electrostatic pDNA polyplexes is one of the key factors in effective transfection. *Colloids Surf., B* **2019**, *184*, 110497.
(16) Maurisse, R.; De Semir, D.; Emamekhoo, H.; Bedayat, B.; Abdolmohammadi, A.; Parsi, H.; Gruenert, D. C. Comparative transfection of DNA into primary and transformed mammalian cells from different lineages. *BMC Biotechnol.* **2010**, *10*, 9.
(17) Bitoque, D. B.; Rosa da Costa, A. M.; Silva, G. A. Insights on the intracellular trafficking of PDMAEMA gene therapy vectors. *Mater. Sci. Eng., C* **2018**, *93*, 277−288.
(18) Zhou, J.; Shao, Z.; Liu, J.; Duan, Q.; Wang, X.; Li, J.; Yang, H. From Endocytosis to Nonendocytosis: The Emerging Era of Gene Delivery. *ACS Appl. Bio Mater.* **2020**, *3*, 2686−2701.
(19) Brock, D. J.; Kondow-McConaghy, H. M.; Hager, E. C.; Pellois, J.-P. Endosomal Escape and Cytosolic Penetration of Macromolecules Mediated by Synthetic Delivery Agents. *Bioconjugate Chem.* **2019**, *30*, 293−304.
(20) Canton, I.; Battaglia, G. Endocytosis at the nanoscale. *Chem. Soc. Rev.* **2012**, *41*, 2718−2739.
(21) Duncan, R.; Richardson, S. C. W. Endocytosis and Intracellular Trafficking as Gateways for Nanomedicine Delivery: Opportunities and Challenges. *Mol. Pharm.* **2012**, *9*, 2380−2402.
(22) Khalil, I. A.; Kogure, K.; Akita, H.; Harashima, H. Uptake pathways and subsequent intracellular trafficking in nonviral gene delivery. *Pharmacol. Rev.* **2006**, *58*, 32−45.
(23) Doherty, G. J.; McMahon, H. T. Mechanisms of Endocytosis. *Annu. Rev. Biochem.* **2009**, *78*, 857−902.
(24) Kaksonen, M.; Roux, A. Mechanisms of clathrin-mediated endocytosis. *Nat. Rev. Mol. Cell Biol.* **2018**, *19*, 313−326.
(25) Sandvig, K.; Kavaliauskiene, S.; Skotland, T. Clathrin-independent endocytosis: an increasing degree of complexity. *Histochem. Cell Biol.* **2018**, *150*, 107−118.
(26) Ita, K. Polyplexes for gene and nucleic acid delivery: Progress and bottlenecks. *Eur. J. Pharm. Sci.* **2020**, *150*, 105358.
(27) Bus, T.; Traeger, A.; Schubert, U. S. The great escape: how cationic polyplexes overcome the endosomal barrier. *J. Mater. Chem. B* **2018**, *6*, 6904−6918.
(28) Behr, J.-P. The proton sponge: a trick to enter cells the viruses did not exploit. *Chimia* **1997**, *51*, 34−36.
(29) Vermeulen, L. M. P.; De Smedt, S. C.; Remaut, K.; Braeckmans, K. The proton sponge hypothesis: Fable or fact? *Eur. J. Pharm. Biopharm.* **2018**, *129*, 184−190.
(30) Guha, S.; Ghimire, J.; Wu, E.; Wimley, W. C. Mechanistic Landscape of Membrane-Permeabilizing Peptides. *Chem. Rev.* **2019**, *119*, 6040−6085.
(31) Dutta, D.; Donaldson, J. G. Search for inhibitors of endocytosis: Intended specificity and unintended consequences. *Cell. Logist.* **2012**, *2*, 203−208.
(32) Rosazza, C.; Deschout, H.; Buntz, A.; Braeckmans, K.; Rols, M.-P.; Zumbusch, A. Endocytosis and Endosomal Trafficking of DNA After Gene Electrotransfer In Vitro. *Mol. Ther.* **2016**, *5*, No. e286.
(33) Sasso, L.; Purdie, L.; Grabowska, A.; Jones, A. T.; Alexander, C. Time and cell-dependent effects of endocytosis inhibitors on the internalization of biomolecule markers and nanomaterials. *J. Interdiscip. Nanomed.* **2018**, *3*, 67−81.
(34) Lechardeur, D.; Verkman, A.; Lukacs, G. Intracellular routing of plasmid DNA during non-viral gene transfer. *Adv. Drug Delivery Rev.* **2005**, *57*, 755−767.
(35) Knockenhauer, K. E.; Schwartz, T. U. The Nuclear Pore Complex as a Flexible and Dynamic Gate. *Cell* **2016**, *164*, 1162−1171.
(36) Bui, K. H.; von Appen, A.; DiGuilio, A. L.; Ori, A.; Sparks, L.; Mackmull, M.-T.; Bock, T.; Hagen, W.; Andrés-Pons, A.; Glavy, J. S.; Beck, M. Integrated Structural Analysis of the Human Nuclear Pore Complex Scaffold. *Cell* **2013**, *155*, 1233−1243.
(37) Grossman, E.; Medalia, O.; Zwerger, M. Functional Architecture of the Nuclear Pore Complex. *Annu. Rev. Biophys.* **2012**, *41*, 557−584.
(38) Maimon, T.; Elad, N.; Dahan, I.; Medalia, O. The Human Nuclear Pore Complex as Revealed by Cryo-Electron Tomography. *Structure* **2012**, *20*, 998−1006.
(39) Bestembayeva, A.; Kramer, A.; Labokha, A. A.; Osmanović, D.; Liashkovich, I.; Orlova, E. V.; Ford, I. J.; Charras, G.; Fassati, A.; Hoogenboom, B. W. Nanoscale stiffness topography reveals structure and mechanics of the transport barrier in intact nuclear pore complexes. *Nat. Nanotechnol.* **2015**, *10*, 60−64.
(40) Sun, M.; Sun, B.; Liu, Y.; Shen, Q.-D.; Jiang, S. Dual-Color Fluorescence Imaging of Magnetic Nanoparticles in Live Cancer Cells Using Conjugated Polymer Probes. *Sci. Rep.* **2016**, *6*, 22368.
(41) Kirchenbuechler, I.; Kirchenbuechler, D.; Elbaum, M. Correlation between cationic lipid-based transfection and cell division. *Exp. Cell Res.* **2016**, *345*, 1.
(42) Lam, A. P.; Dean, D. A. Progress and prospects: nuclear import of nonviral vectors. *Gene Ther.* **2010**, *17*, 439−447.
(43) Bai, H.; Lester, G. M. S.; Petishnok, L. C.; Dean, D. A. Cytoplasmic transport and nuclear import of plasmid DNA. *Biosci. Rep.* **2017**, *37*, BSR20160616.
(44) Sun, Y.; Xian, L.; Xing, H.; Yu, J.; Yang, Z.; Yang, T.; Yang, L.; Ding, P. Factors influencing the nuclear targeting ability of nuclear localization signals. *J. Drug Targeting* **2016**, *24*, 927−933.
(45) Sola, B.; Staedel, C.; Remy, J.-S.; Bahr, A.; Behr, J.-P. Lipospermine-mediated gene transfer technique into murine cultured cortical cells. *J. Neurosci. Methods* **1997**, *71*, 183−186.
(46) Bishop, C. J.; Majewski, R. L.; Guiriba, T.-R. M.; Wilson, D. R.; Bhise, N. S.; Quiñones-Hinojosa, A.; Green, J. J. Quantification of cellular and nuclear uptake rates of polymeric gene delivery nanoparticles and DNA plasmids via flow cytometry. *Acta Biomater.* **2016**, *37*, 120−130.
(47) Tasharrofi, N.; Kouhkan, F.; Soleimani, M.; Soheili, Z.-S.; Atyabi, F.; Akbari Javar, H.; Abedin Dorkoosh, F. Efficient gene delivery to primary human retinal pigment epithelial cells: The innate and acquired properties of vectors. *Int. J. Pharm.* **2017**, *518*, 66−79.

https://dx.doi.org/10.1021/acsomega.0c03367
ACS Omega 2020, 5, 26640−26654

(48) Chen, J.; Hessler, J. A.; Putchakayala, K.; Panama, B. K.; Khan, D. P.; Hong, S.; Mullen, D. G.; DiMaggio, S. C.; Som, A.; Tew, G. N.; Lopatin, A. N.; Baker, J. R.; Holl, M. M. B.; Orr, B. G. Cationic Nanoparticles Induce Nanoscale Disruption in Living Cell Plasma Membranes. *J. Phys. Chem. B* **2009**, *113*, 11179−11185.
(49) Hong, S.; Bielinska, A. U.; Mecke, A.; Keszler, B.; Beals, J. L.; Shi, X.; Balogh, L.; Orr, B. G.; Baker, J. R.; Banaszak Holl, M. M. Interaction of Poly(amidoamine) Dendrimers with Supported Lipid Bilayers and Cells: Hole Formation and the Relation to Transport. *Bioconjugate Chem.* **2004**, *15*, 774−782.
(50) Mecke, A.; Majoros, I. J.; Patri, A. K.; Baker, J. R.; Banaszak Holl, M. M.; Orr, B. G. Lipid Bilayer Disruption by Polycationic Polymers: The Roles of Size and Chemical Functional Group. *Langmuir* **2005**, *21*, 10348−10354.
(51) Leroueil, P. R.; Berry, S. A.; Duthie, K.; Han, G.; Rotello, V. M.; McNerny, D. Q.; Baker, J. R.; Orr, B. G.; Banaszak Holl, M. M. Wide varieties of cationic nanoparticles induce defects in supported lipid bilayers. *Nano Lett.* **2008**, *8*, 420−424.
(52) Harrisson, F.; Callebaut, M.; Vakaet, L. Microspectrographic analysis of trypan blue-induced fluorescence in oocytes of the Japanese quail. *Histochemistry* **1981**, *72*, 563−578.
(53) Darzynkiewicz, Z. Critical aspects in analysis of cellular DNA content. *Curr. Protoc. Cytom.* **2011**, *56*, 7.2.1.
(54) Avelar-Freitas, B. A.; Almeida, V. G.; Pinto, M. C. X.; Mourão, F. A. G.; Massensini, A. R.; Martins-Filho, O. A.; Rocha-Vieira, E.; Brito-Melo, G. E. A. Trypan blue exclusion assay by flow cytometry. *Braz. J. Med. Biol. Res.* **2014**, *47*, 307−315.
(55) Bäckström, A.; Kugel, L.; Gnann, C.; Xu, H.; Aslan, J. E.; Lundberg, E.; Stadler, C. A sample preparation protocol for high throughput immunofluorescence of suspension cells. **2020**, bioRxiv:2020.01.05.895201.
(56) Raup, A.; Wang, H.; Synatschke, C. V.; Jérôme, V.; Agarwal, S.; Pergushov, D. V.; Müller, A. H. E.; Freitag, R. Compaction and Transmembrane Delivery of pDNA: Differences between l-PEI and Two Types of Amphiphilic Block Copolymers. *Biomacromolecules* **2017**, *18*, 808−818.
(57) Zakharova, S. S.; Jesse, W.; Backendorf, C.; Egelhaaf, S. U.; Lapp, A.; van der Maarel, J. R. C. Dimensions of Plectonemically Supercoiled DNA. *Biophys. J.* **2002**, *83*, 1106−1118.
(58) Schallon, A.; Synatschke, C. V.; Pergushov, D. V.; Jérôme, V.; Müller, A. H. E.; Freitag, R. DNA melting temperature assay for assessing the stability of DNA polyplexes intended for nonviral gene delivery. *Langmuir* **2011**, *27*, 12042−12051.
(59) Bourzac, K. M.; LaVine, L. J.; Rice, M. S. Analysis of DAPI and SYBR Green I as Alternatives to Ethidium Bromide for Nucleic Acid Staining in Agarose Gel Electrophoresis. *J. Chem. Educ.* **2003**, *80*, 1292−1297.
(60) Crissman, H. A.; Oka, M. S.; Steinkamp, J. A. Rapid staining methods for analysis of deoxyribonucleic acid and protein in mammalian cells. *J. Histochem. Cytochem.* **1976**, *24*, 64−71.
(61) Toba, K.; Winton, E. F.; Koike, T.; Shibata, A. Simultaneous three-color analysis of the surface phenotype and DNA-RNA quantitation using 7-amino-actinomycin D and pyronin Y. *J. Immunol. Methods* **1995**, *182*, 193−207.
(62) Dubruel, P.; Christiaens, B.; Vanloo, B.; Bracke, K.; Rosseneu, M.; Vandekerckhove, J.; Schacht, E. Physicochemical and biological evaluation of cationic polymethacrylates as vectors for gene delivery. *Eur. J. Pharm. Sci.* **2003**, *18*, 211−220.
(63) Schmid, I.; Cole, S. W.; Korin, Y. D.; Zack, J. A.; Giorgi, J. V. Detection of cell cycle subcompartments by flow cytometric estimation of DNA-RNA content in combination with dual-color immunofluorescence. *Cytometry* **2000**, *39*, 108−116.
(64) Chen, B.; Synatschke, C. V.; Jérôme, V.; Müller, A. H. E.; Freitag, R.; Wu, C. Co-transfection of star-shaped PDMAEMAs enhance transfection efficiency of protamine/pDNA complexes in the presence of serum. *Eur. Polym. J.* **2018**, *103*, 362−369.
(65) Plamper, F. A.; Schmalz, A.; Penott-Chang, E.; Drechsler, M.; Jusufi, A.; Ballauff, M.; Müller, A. H. E. Synthesis and Characterization of Star-Shaped Poly(N,N-dimethylaminoethyl methacrylate) and Its Quaternized Ammonium Salts. *Macromolecules* **2007**, *40*, 5689−5697.
(66) Diaz, I. L.; Sierra, C. A.; Jérôme, V.; Freitag, R.; Perez, L. D. Target grafting of poly(2-(dimethylamino)ethyl methacrylate) to biodegradable block copolymers. *J. Polym. Sci.* **2020**, *58*, 2168−2180.

https://dx.doi.org/10.1021/acsomega.0c03367
ACS Omega 2020, 5, 26640−26654